Original Article

Podoplanin promotes cancer-associated thrombosis and contributes to the unfavorable overall survival in an ectopic xenograft mouse model of oral cancer

Hsing-Ying Lee [a], Ni-Yen Yu [b], Shiang-Hsuan Lee [b], Hui-Ju Tsai [b], Chih-Ching Wu [b,c], Ju-Chien Cheng [d], Ding-Ping Chen [a,b,e], Ying-Ru Wang [f], Ching-Ping Tseng [a,b,e,f,g,*]

[a] Graduate Institute of Biomedical Sciences, College of Medicine, Chang Gung University, Taoyuan, Taiwan
[b] Department of Medical Biotechnology and Laboratory Science, College of Medicine, Chang Gung University, Taoyuan, Taiwan
[c] Department of Otolaryngology-Head & Neck Surgery, Chang Gung Memorial Hospital at Linkou, Taoyuan, Taiwan
[d] Department of Medical Laboratory Science and Biotechnology, China Medical University, Taichung, Taiwan
[e] Department of Laboratory Medicine, Chang Gung Memorial Hospital at Linkou, Taoyuan, Taiwan
[f] Graduate Institute of Medical Biotechnology and Laboratory Science, College of Medicine, Chang Gung University, Taoyuan, Taiwan
[g] Molecular Medicine Research Center, Chang Gung University, Taoyuan, Taiwan

ARTICLE INFO

ABSTRACT

Background: Podoplanin (PDPN) is a transmembrane glycoprotein that mediates tumor cell-induced platelets aggregation in different cancer types. Emerging data indicate that PDPN is a marker for poor prognosis of human oral squamous cell carcinoma (OSCC). However, the functional impacts of PDPN on cancer formation and disease progression of OSCC remain to be elucidated.

Methods: The sublines of the OECM-1 oral cancer cells with PDPN knockdown or over-expression were established. The cellular characteristics and the ability to induce platelet aggregation of these cells lines were analyzed. An ectopic xenograft animal model by inoculating cancer cells into the anterior neck region of nude mice was established to investigate the functional impact of PDPN on disease progression and cancer-associated thrombosis of OSCC.

Results: PDPN promoted OSCC cell migration and invasion, but had no effect on cell proliferation *in vitro* and tumor growth *in vivo*. Co-incubation of PDPN-positive (PDPN$^+$) OSCC cells with platelets induced platelet activation and aggregation. The mice bearing PDPN$^+$ tumor had a decrease in overall survival despite that there was no gross appearance of distant metastasis. A speckled immunofluorescence staining pattern of platelet marker

mCD41 was defined in the PDPN⁺ tumor sections and the intensity was greater than in the PDPN-low or negative tumor sections. Co-immunofluorescence staining of the tumor sections with mCD41 and the endothelial cell marker mCD31 further demonstrated that platelet aggregates were located in the lumen of blood vessel and were also distributed intratumorally in the mice bearing PDPN⁺ tumors.

Conclusions: These data demonstrated that PDPN expression in the cancer cells is associated with high risk of thrombosis, leading to unfavorable overall survival of the mice. This study provides new insights into the functions of PDPN in cancer-associated thrombosis and in the pathophysiology of OSCC.

At a glance of commentary

Scientific background on the subject

Cancer-associated thrombosis is one of the major causes of death in patients with oral cancer and is an emerging issue to investigate. An ectopic xenograft mouse model was established to address whether podoplanin expression links to an increase in thrombotic risk and disease progression of oral cancer.

What this study adds to the field

Podoplanin expression in oral cancer is associated with unfavorable overall survival. Cancer-associated thrombosis but not distant metastasis contributes to the effects of podoplanin on the poor prognosis of animals. This study provides new insights into the functions of podoplanin in cancer-associated thrombosis and in the pathophysiology of oral cancer.

Oral squamous cell carcinoma (OSCC) is a life-threatening disease with an estimated 202,000 newly diagnosed cases annually. Papillomavirus infection and the consumption of tobacco, alcohol and areca nut are the major etiological factors for the initiation and promotion of OSCC cells [1]. Despite the advancement of surgery and radiation therapy, the overall survival of patients is not improved significantly during the past decades. Distant metastasis and locally advanced disease with cancer cells infiltrating into lymph nodes contribute mainly to the death of patients with OSCC [2]. There is an unmet need to illustrate the cellular properties of cancer cells and the mechanistic insight attributing to disease progression of OSCC.

The 38—40 KDa transmembrane glycoprotein Podoplanin (PDPN), which induces platelet aggregation by binding to the platelet C-type lectin-like receptor 2 (CLEC-2) [3,4], is among the most frequently upregulated genes in OSCC cells [5]. Under physiological condition, PDPN regulates blood-lymphatic vessel separation [6], cerebrovascular patterning and integrity [7], the maintenance and integrity of high endothelial venules in lymph nodes [8], megakaryocyte proliferation, proplatelet formation [9], wound healing [10], and efficient T-cell priming [11]. In the pathological condition such as cancer, PDPN is implicated in the progression of squamous cell carcinoma, mesothelioma, testicular seminoma, and brain tumors [12]. With protein expression mainly in the invasive front of tumor, PDPN promotes cancer progression by increasing cell spreading and collective and single cell migration and invasion [13], induction of RhoA activity and modulation of actin cytoskeleton [13,14].

Most PDPN studies in OSCC also indicate that PDPN is involved in tumor invasion, cell migration, cell adhesion to extracellular matrix [15], and functional invadopodia formation [16]. In the clinical aspects, PDPN expression correlates with tumor lymphangiogenesis, lymph node metastasis [17], less response to neoadjuvant chemoradiotherapy [18], and poor clinical outcome of patients with OSCC [19,20]. The relative number of circulating tumor cells (CTCs) expressing PDPN and epithelial cell adhesion molecule also correlates with poor progression-free survival and overall survival of cancer patients [21]. However, whether or not PDPN induces cancer-associated thrombosis contributing to the pathogenesis of OSCC has not yet been elucidated.

Acquiring platelet aggregation activity by platelet mimicry and expression of proteins capable of inducing platelet aggregation represent the hallmarks of cancer cells with hematogenous dissemination [22]. With the capability of inducing platelet aggregation, PDPN enhances metastatic foci formation in the lung and decreases the overall survival of the animals when CHO cells overexpressing PDPN were injected intravenously into the nude mice [3]. PDPN-Fc fusion protein generated in the transgenic mice under the control of keratin 14 promoter enters the bloodstream and induces disseminated intravascular coagulation [23]. Intravascular thrombosis and increased risk of venous thromboembolism have also been reported in patients with brain tumors expressing PDPN [24]. However, there is still a lack of *in vivo* animal study to confirm the link between PDPN expression in the cancer cells and thrombotic risk, which were addressed in this study.

We demonstrated that PDPN promoted OSCC cell migration and invasion *in vitro*, but had no effect on cell proliferation *in vitro* and tumor growth in an ectopic xenograft nude mouse model. Notably, OSCC cells with PDPN expression caused an increase in intravascular platelet aggregation and platelet infiltration to the OSCC tumors contributing to the poor survival of mice. The findings of this study provide new insights into the functions of PDPN in cancer-associated thrombosis and in the pathophysiology of OSCC.

Material and methods

Ethical statement

The use of human platelets in this study was approved by the Institutional Review Board (IRB) of Chang Gung Memorial Hospital (CGMH). All experiments were performed in accordance with the guidelines and regulations by the IRB at CGMH. Prior to sample collection, written informed consent was obtained from all volunteers. The animal protocol was reviewed and approved by the Institutional Animal Care and Use Committee of the Laboratory Animal Center, Chang Gung University, in accordance with the guidelines of the Animal Welfare and Animal Protection Law of Council of Agriculture, Taiwan.

Materials

The culture medium, Lipofectamine™ 2000 reagent, Cell-Trace™ Calcein Red-Orange, AM, Calcein, AM and rat anti-mouse CD41 (mCD41) antibody were purchased from Thermo Fisher Scientific (Waltham, Massachusetts, USA). BD Matrigel™ basement membrane matrix was purchased from BD Bioscience (San Jose, CA, USA). Rat anti-human PDPN antibody (NZ-1) was purchased from AngioBio (San Diego, CA, USA). Fluorescein isothiocyanate (FITC)-conjugated goat anti-rat antibody, Alexa Fluor 488 (AF488)-conjugated rat anti-human PDPN (NC-08) antibody, AF488-conjugated rat IgG$_2$ antibody, phycoerythrin (PE)-conjugated anti-human CD62P (p-selectin) antibody, PE-conjugated anti-mouse IgG$_1$ antibody, biotin-conjugated anti-mouse Ter119 antibody, Mojo-Sort™ streptavidin nanobeads, and MojoSort™ mouse CD45 nanobeads were purchased from BioLegend (San Diego, CA, USA). Rabbit anti-mouse CD31 (mCD31) antibody and the mouse thrombin-anti-thrombin (TAT) complexes enzyme-linked immunosorbent assay (ELISA) kit were purchased from Abcam (Cambridge, UK). The anti-human PDPN monoclonal antibody (LpMab-12), which specifically binds to the glycosylated Thr52, was a kind gift from Professor Yukinari Kato (Tohoku University School of Medicine, Sendai, Miyagi, Japan). The *in vivo* grade VivoGlo™ Luciferin was purchased from Promega (Madison, Wisconsin, USA). ASSERACHROM®

D-DI ELISA kit was purchased from Stago (Asnières sur Seine, France). The rabbit anti-fibrin(ogen) antibody was purchased from Agilent (Santa Clara, California, USA). The mouse anti-human β-actin monoclonal antibody, Hoechst 33342 and KAPA2G Robust PCR kit were purchased from Sigma–Aldrich (St. Louis, Missouri, USA). The lentivirus-based short hairpin RNA (shRNA) plasmids targeting on β-galactosidase and PDPN were purchased from the RNAi Core Lab of Academia Sinica (Taiwan).

Cell culture

Oral cancer cell lines Ca9-22, SAS and CAL27 were maintained in Dulbecco's Modified Eagle's medium (DMEM) supplemented with 1% glutamate. The OECM-1 and OC2 cells were maintained in Roswell Park Memorial Institute 1640 (RPMI-1640) medium. The TW2.6, HSC-3 and SCC-4 cells were maintained in DMEM/F-12 medium. HEK-293T cells were maintained in DMEM. All aforementioned culture media were supplemented with 10% fetal bovine serum (FBS) and 1% penicillin-streptomycin (P/S) solution. OC3 cells were maintained in keratinocyte serum-free medium and DMEM/10% FBS (2:1 ratio) supplemented with 1% P/S solution. The origin and the relative information of these OSCC cell lines were described in [Table 1]. C6-lung, a subline of rat glioblastoma C6 cells collected from cells metastasizing to lung [25], was maintained in Ham's F-12K medium supplemented with 2.5% horse serum, 10% FBS and 1% P/S solution. All cells were maintained in a humidified atmosphere at 37 °C with 5% CO$_2$.

Cell growth assay

Cells were seeded into the 6-well culture plate at the density of 5×10^4 cells/well. At the indicated time points, the cells were harvested by trypsinization and the cell suspension was mixed with trypan blue for counting using the hemocytometer.

Flow cytometry analysis

For fluorescence-activated cell sorting (FACS), OECM-1 cells were immunostained with the rat anti-human PDPN antibody

Table 1 The oral cancer cell lines used in this study.							
Cell line	Cancerous tissue	Isolated from	Donor information				
			Sex	Age	Country	Areca nut chewing	Smoking
Ca9-22	Gingiva	Primary site	M	n.a.	Japan	n.a.	n.a.
OECM-1	Gingiva	Primary site	M	n.a.	Taiwan	Yes	No
OC2	Buccal mucosa	Metastatic site	M	51	Taiwan	Yes	Yes
OC3	Buccal mucosa	Primary site	M	n.a.	Taiwan	Yes	No
TW2.6	Buccal mucosa	Primary site	M	48	Taiwan	Yes	Yes
HSC-3	Tongue	Metastatic site	M	64	Japan	n.a.	n.a.
SAS	Tongue	Primary site	n.a.	n.a.	Japan	n.a.	n.a.
SCC-4	Tongue	Primary site	M	56	USA	n.a.	n.a.
CAL27	Tongue	Primary site	M	56	France	n.a.	n.a.
Abbreviation: n.a.: not available.							

(NZ-1) followed by FITC-conjugated goat anti-rat antibody. The cells were re-suspended in 1X phosphate-buffered saline (PBS) for cell sorting using FACSAria II Cell Sorter (BD Bioscience, San Jose, CA, USA). The cells with high PDPN expression (top 20%) and the PDPN-negative cells were collected and cultured to form the P^+ and P^- sublines, respectively.

For analysis of cell surface PDPN expression, the cells were immunostained with AF488-conjugated rat anti-human PDPN antibody. Surface expression of platelet activation marker CD62P (P-selectin) was analyzed by immunostaining the cancer cell-platelet mixed aggregates with PE-conjugated mouse anti-human CD62P antibody. Immunostaining with the AF488-conjugated rat IgG_2 antibody or PE-conjugated mouse IgG_1 was used as the negative control, respectively. These samples were analyzed by using BD Accuri™ C6 Cytometer (BD Bioscience, San Jose, CA, USA).

Generation of recombinant lentiviruses

HEK-293T cells (2×10^6) were seeded into a 6-cm culture dish for 24 h followed by co-transfection of 4 μg of HIV-1-based lentiviral packaging plasmid pCMVδ 8.91, 0.4 μg of VSV-G expression plasmid pMD.G, and 4 μg of lentivirus expression plasmids using the Lipofectamine 2000 reagent. The lentivirus expression plasmids encoded either *luciferase*, human *PDPN*, shRNA targeting on *β-galactosidase* (shLacZ: 5′-TGTTCGCAT-TATCCGAACCAT-3′) which was not expressed in the eukaryotic cells, or shRNA targeting on human PDPN (shPDPN clone 1: 5′-CAACAACTCAACGGGAACGAT-3′; and shPDPN clone 7: 5′-GCAACAAGTGTCAACAGTGTA-3′). The cell medium was replaced with fresh DMEM supplemented with 10% FBS at 5 h post-transfection. The supernatants containing the lentiviral particles were harvested at 24 h and 48 h post-transfection. After passing through a 0.22-μm filter, the lentiviral particles were aliquot and stored at −80 °C until use.

Establish P^+ and P^- sublines with luciferase *gene expression*

The P^+ and P^- cells were seeded into a 6-well tissue culture plate (2×10^5 cells/well) and were infected the following day with the recombinant lentivirus encoding luciferase mRNA (24 h and 48 h viral supernatants in a 1:1 ratio) in RPMI-1640 supplemented with 10% FBS and 8 μg/ml of protamine sulfate. The virus-containing medium was replaced with fresh RPMI-1640 supplemented with 10% FBS at 12 h post-infection. At 48 h after viral infection, the cells were cultured in RPMI-1640 containing 100 μg/ml hygromycin for two weeks to select for P^+Luc^+ and P^-Luc^+ cells which were P^+ and P^- cells expressing *luciferase* gene, respectively.

Generation of luciferase-expressing P^+ and P^- sublines with knockdown or overexpression of PDPN

P^+Luc^+ cells were infected with the recombinant lentiviruses encoding shLacZ, shPDPN1 and shPDPN7, respectively, by the protocols as described in previous section. At 48 h after viral infection, cells were cultured in RPMI-1640 containing 4 μg/ml puromycin for two weeks to select for P^+Luc^+ cells with PDPN

knockdown (P^+-shPDPN1 and P^+-shPDPN7) and their corresponding control (P^+-shLacZ) cells. On the other hand, the P^+Luc^+ and P^-Luc^+ cells were infected with the recombinant viruses carrying human PDPN cDNA or vector control to establish PDPN-overexpressing (P^+-PDPN and P^--PDPN) and vector control (P^+-vector and P^--vector) cells. Noted that all sublines with PDPN knockdown or overexpression were *luciferase*-positive. For simplicity purpose, "Luc^+" was omitted for the nomenclature of these sublines.

Human washed platelet preparation

The peripheral blood of healthy volunteers was drawn into a collection tube containing 3.18% sodium citrate in a ratio of 9:1. Washed platelets were prepared as described previously [26] and were re-suspended in Tyrode's buffer (137 mM NaCl, 2.65 mM KCl, 12 mM $NaHCO_3$, 0.43 mM NaH_2PO_4, 2 mM $CaCl_2$, 1 mM $MgCl_2$, 5 mM glucose, 5 mM HEPES, pH 7.35, and 0.35% bovine serum albumin) to a final concentration of 1×10^9/ml.

Western blot analysis

Protein lysates were prepared as described previously [27]. Fifteen μg of the protein lysates were fractionated on a 10% SDS-PAGE and electrotransferred onto a polyvinylidene difluoride membrane. After blocking the membrane with 5% fat-free milk prepared in 1X PBS containing 0.1% Tween 20 (PBST) for 30 min, the membrane was incubated with the indicated primary antibody for 1.5 h. After washing with 1X PBST, the membrane was incubated with the horseradish peroxidase (HRP)-conjugated secondary antibody (1:10000) for 1 h. Specific protein bands were detected by using the Millipore Immobilon Western Chemiluminescent HRP substrate (Millipore, Burlington, MA, USA). The band intensity was quantified by ImageJ software (National Institute of Health).

Migration and invasion assay

Transwell was used for cell migration and invasion assays. The transwell membrane was pre-coated with 5% matrigel for invasion assay. The cells (1×10^5) in 300 μl of RPMI-1640 medium containing 1% FBS were seeded on the upper well of the transwell, while 600 μl of RPMI-1640 medium containing 20% FBS was added into the lower chamber. After incubation for the indicated time, the transwell was washed with 1X PBS and the cells were fixed with 100% methanol for 10 min. Giemsa stain was used for cell staining. Cells adhered to the upper surface of the membrane were carefully removed by cotton swab. The images of each transwell membrane were examined and acquired by using a Zeiss Primo Star microscope (Carl Zeiss, Gottingen, Germany) with 100X magnification. The number of migrated and invaded cells on the transwell membrane was counted manually.

Tumor cell-induced platelet aggregation (TCIPA)

Washed platelets (480 μl with the density of 1 X 10^9 platelets/ml) were incubated in an aggregometer (Chrono-Log Corp., Havertown, PA, USA) at a constant stirring (37 °C, 900 rpm) for

2 min. Platelet aggregation was induced by adding 20 μl of cancer cells (1×10^6 or 3×10^6). Platelet aggregation pattern was recorded for 30 min using the Aggro/Link processing software (Chrono-Log Corp., Havertown, PA, USA). For observations of tumor cell-platelet mixed aggregates under fluorescence microscopy, platelets and cancer cells were pre-labeled with CellTrace™ Calcein Red-Orange AM (red) and Calcein AM (green), respectively. After mixing cancer cells and platelets under constant stirring at 900 rpm, the reaction mixtures were placed on a slide and were observed by the Zeiss Axiovert 200M fluorescence microscopy (Carl Zeiss, Gottingen, Germany) at 100X magnification.

Ectopic xenograft mouse model

The OECM-1 cells (1×10^6 in 100 μl 1X PBS) were inoculated into the anterior neck region of nude mice. The body weight of nude mice was recorded every 2–3 days. The survival time was monitored for 50 days. During the period of experiment, the tumor size was monitored by using the *In vivo* imaging system (IVIS)-200 (Xenogene cooperation, Berkeley, CA, USA). In this regard, the mice were first anesthetized by inhalation of 2.5% isoflurane for 5 min and were subcutaneously injected with D-luciferin (150 mg/kg) to the dorsal midline, midway between the head and tail of the mouse. The images were acquired 8 min post-D-luciferin injection. The sum of luminescence intensity of the region of interest was determined.

Isolation of CTCs

Isolation of CTCs from mouse blood was performed by using the modified PowerMag system [28], which has been established and validated in our previous study. Mouse blood was collected into a tube containing the anticoagulant, K_2-EDTA, via cardiac puncture. Erythrocytes were lysed by mixing whole blood with RBC lysis buffer (0.15 M NH_4Cl and 10 mM $NaHCO_3$) in the ratio of 1:10 for 5 min at room temperature. After centrifugation for 3 min, the cell pellets were resuspended in 1 ml of cell culture medium and the erythrocytes lysis step was performed one more time. The nucleated cells were then washed and subsequently resuspended in 100 μl of cell culture medium. The MojoSort™ mouse CD45 nanobeads and the biotin anti-mouse Ter119 antibody were mixed with the collected cell pellets and incubate at room temperature for 15 min. The mixture was then loaded into the PowerMag column to deplete CD45$^+$-leukocytes and the remaining erythrocytes. Cell eluates were collected for further analysis.

Detection of CTCs by PCR

The presence of genomic DNA containing the *luciferase* gene fragment in the cell eluates was used as an indicator for the existence of CTCs in the peripheral blood of mice bearing *luciferase*-expressing OECM-1 tumor. Briefly, PCR was performed to amplify the *luciferase* gene fragment in a 40 μl reaction mixtures containing 18 μl of cell eluates lysed by sonication, 1X KAPA2G Buffer A, 1X KAPA Enhancer 1, 0.2 mM

dNTPs, 0.5 μM Luc forward primer (5′-CAACTGCATAAGGCTATGAAGAGA-3′), 0.5 μM Luc reverse primer (5′-ATTTGTATTCAGCCCATATCGTTT -3′), and 0.5 U KAP2G Robust DNA polymerase. The cycling condition was 1 cycle at 95 °C for 3 min, 50 cycles at 95 °C for 15 s, 60 °C for 15 s, and 72 °C for 15 s, followed by 1 cycle at 72 °C for 2 min. The length for the PCR product of *luciferase* gene is 153 base pair.

Thrombin-anti-thrombin (TAT) complex and D-dimer ELISA assay

Mouse blood was collected into a tube containing the anticoagulant sodium citrate via cardiac puncture (blood: 3.18% sodium citrate = 9:1). Plasma was collected by centrifugation of whole blood at 3000 g for 10 min and was subject to TAT and D-dimer assays using the TAT Complexes Mouse ELISA kit and ASSERACHROM® D-DI ELISA kit, respectively, as described by the manufacturers.

Fibrin(ogen) deposition analysis by immunohistochemistry

For analysis of fibrin(ogen) deposition in the blood vessel, lung and kidney of the tumor-bearing mice were fixed with 10% neutral-buffered formalin overnight and embedded in paraffin. The paraffin-embedded sections (5 μm) on the slides were subject to dewaxing, hydration and heat-induced epitope retrieval by using 1X Trilogy pretreatment solution (Cell Marque, Rocklin, CA, USA). After rinsing in 1X Tris-buffered saline with 0.1% Tween 20 (TBST), the slides were incubated with 3% H_2O_2 for 10 min to inhibit the activity of endogenous peroxidase and Rodent Block M for 2 h to block non-specific antibody binding. The slides were then incubated with primary anti-fibrin(ogen) antibody (1:500) at 4 °C overnight. After washing with 1X TBST several times, the slides were incubated with HRP-conjugated anti-rabbit antibody (1:500) at room temperature for 1 h. After several washes with 1X TBST, the slides were incubated with 3,3′-diaminobenzidine for immunohistochemical staining followed by counterstaining with hematoxylin. The sections were mounted and the images were acquired by using a Zeiss Primo Star microscope (Carl Zeiss, Gottingen, Germany). The quantitative data of fibrin(ogen) positive pulmonary vasculature were acquired by analysis of 40–50 high power field (200X) images obtained from 5 mice in each group.

Immunofluorescence staining

For immunofluorescence staining, tissue cryosections (5 μm) were fixed in CellCover fixation buffer for 30 min, and then blocked with Rodent Block M prepared in 1X TBST for 1 h. The tissue sections were incubated with the rat anti-human PDPN antibody (NZ-1) (1:50), the rat anti-mCD41 antibody (1:100) or the rabbit anti-mCD31 antibody (1:100) for 1 h followed by the AF555-conjugated goat anti-rat antibody (1:250, for PDPN and mCD41) or the AF488-conjugated goat anti-rabbit antibody (1:300, for mCD31). The nuclei were counterstained with Hoechst 33342 for 1 h. The sections were mounted in

fluorescent mounting medium and the fluorescence signal was determined by fluorescence microscopy Zeiss Axiovert 200M (Carl Zeiss, Gottingen, Germany) at 100X magnification. For quantification of fluorescent signals, images of the whole cryosection were acquired by using the IN Cell Analyzer 1000 (GE Healthcare, England). The average fluorescence intensity of the target protein per unit area of the tissue section was then determined by using the software of IN Cell Investigator (GE Healthcare, England).

Statistical analysis

IBM SPSS Statistics V22.0 (Armonk, New York, USA) and Prism version 5.0 (San Diego, CA, USA) software packages were used for statistical analysis. Animal survival analysis was performed by using the Kaplan—Meier survival curve followed by log-rank test. The *in vivo* assays were analyzed by nonparametric methods. The fluorescence signals of tumor sections, the data of TAT and D-dimer assays and the immunohistochemistry assay were analyzed by the

Mann—Whitney U-test; the platelet counts and MPV were analyzed by the Kruskal—Wallis test. All *in vitro* experiments were analyzed by the parametric unpaired Student's t-test or one-way ANOVA. Data were considered statistically significant when $p < 0.05$.

Results

Establish a PDPN knockdown cell model for studying the role of PDPN in disease progression of OSCC

The cell lysates of nine OSCC cell lines derived from the gingiva (Ca9-22 and OECM-1), the buccal mucosa (OC2, OC3 and TW2.6), and the tongue (HSC-3, SAS, SCC-4 and CAL27) were analyzed by Western blot to determine the expression levels of PDPN in OSCC cells [Fig. 1A]. PDPN was expressed in five of the nine cell lines including OECM-1, OC2, TW2.6, HSC-3, and CAL27. A slightly different molecular mass of 45—55 kDa was noted among these cell lines. It is likely that PDPN undergoes various
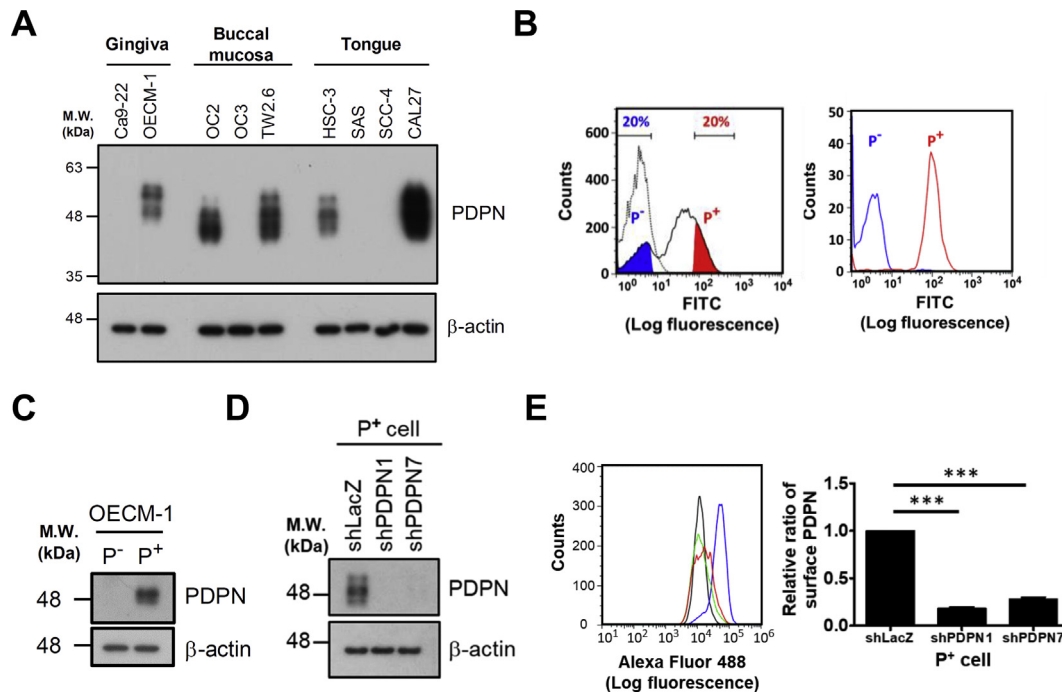

Fig. 1 **Characterization of PDPN expression in the OSCC cell lines**. (A) The lysates of the indicated cell lines were analyzed by Western blot using the anti-PDPN (NZ-1) antibody and anti-β-actin antibody, respectively. (B) OECM-1 cells were labeled with rat anti-human PDPN antibody followed by FITC-conjugated anti-rat antibody and subjected to cell sorting using the FACSAria cell sorter. The cells with high PDPN expression (top 20%; red) and the PDPN-negative cells (blue) were collected and designated as P⁺ and P⁻ cells, respectively. Isotype control (dot line) was used as a negative control to define the fluorescence signal without PDPN expression (left panel). PDPN expression of the sorted P⁻ and P⁺ cells were re-analyzed immediately by flow cytometry after sorting (right panel). (C) PDPN expression in the P⁻ and P⁺ cells was analyzed by Western blot using the anti-PDPN (NZ-1) antibody. The expression of β-actin was used as the loading control. (D) PDPN expression in the P⁺-shLacZ, P⁺-shPDPN1 and P⁺-shPDPN7 cells was analyzed by Western blot. (E) The cell surface of P⁺-shLacZ, P⁺-shPDPN1, and P⁺-shPDPN7 sublines was labeled with Alexa Fluor 488-conjugated anti-PDPN antibody or the isotype control (incubated with P⁺-shLacZ cells) followed by flow cytometry. The histogram representing the fluorescence intensity of the indicated cells is shown (left panel). (Blue: P⁺-shLacZ; green: P⁺-shPDPN1; red: P⁺-shPDPN7; black: isotype control) The mean fluorescence intensity (MFI) for the indicated cells was determined and used as an indicator of PDPN expression on the cell surface. The relative ratio of surface PDPN expression is shown with PDPN on the cell surface of P⁺-shLacZ arbitrarily set as 1 (right panel). The mean ± SEM of 3 independent experiments is shown. ***, $p < 0.001$.

post-translational modifications such as glycosylation and phosphorylation [29,30] in different cell lines.

Most of the oral cancer in Taiwan is related to the consuming of areca nut which is not common in Western country. Among the PDPN-expressing cell lines isolated from patients with history of areca nut chewing (OECM-1, TW2.6, and OC2), OECM-1 was the most commonly used cell model [31,32] for investigating oral cancer pathogenesis and therefore was selected for our study. Flow cytometry analysis of cell surface PDPN revealed that PDPN was not homogenously expressed on each individual OCEM-1 cell. Some cells expressed high levels of PDPN, while the others had no detectable PDPN. OECM-1 cells with high PDPN expression (top 20%) and the PDPN-negative cells were collected by cell sorting and were cultured as the P^+ and P^- cells, respectively. The levels of PDPN expression for P^+ and P^- cells were confirmed by re-analyzing the cells immediately after sorting [Fig. 1B]. Western blot analysis of the cell lysates from these two populations of OECM-1 cells showed that PDPN was highly expressed in P^+ cells, but minimally or not expressed in P^- cells [Fig. 1C]. There was no difference in cell morphology between P^+ and P^- cells (see Supplementary Fig. S1A). PDPN expression in P^+ cells and the phenotype of the P^+ and P^- cells were stable throughout the study.

P^+ subline with *luciferase* expression was first generated by infection of P^+ cells with recombinant lentiviruses carrying *luciferase* gene. The control P^+-shLacZ cells and the PDPN knockdown sublines (P^+-shPDPN1 and P^+-shPDPN7) were established by infecting *luciferase*-expressing P^+ cells with recombinant lentiviruses carrying shRNA targeting on the mRNA sequences of β-galactosidase and PDPN, respectively. Western blot analysis of the cell lysates from these sublines revealed that PDPN expression was diminished in P^+-shPDPN1 and P^+-shPDPN7 cells when compared to P^+-shLacZ cells [Fig. 1D]. These data are consistent with the findings of flow cytometry analysis, showing that cell surface expression of PDPN for P^+-shPDPN1 and P^+-shPDPN7 cells was $18.3 \pm 2.5\%$ and $28.0 \pm 3.6\%$ of P^+-shLacZ cells, respectively ($p < 0.001$) [Fig. 1E]. There was no difference in cell morphology among P^+-shLacZ, P^+-shPDPN1, and P^+-shPDPN7 cells (see Supplementary Fig. S1B).

Effects of PDPN knockdown on cellular properties and *in vitro* platelet aggregation activity of OSCC cells

The effects of PDPN knockdown on the cellular properties of OSCC cells were characterized in the following experiments. Cell growth rate was comparable among P^+-shLacZ, P^+-
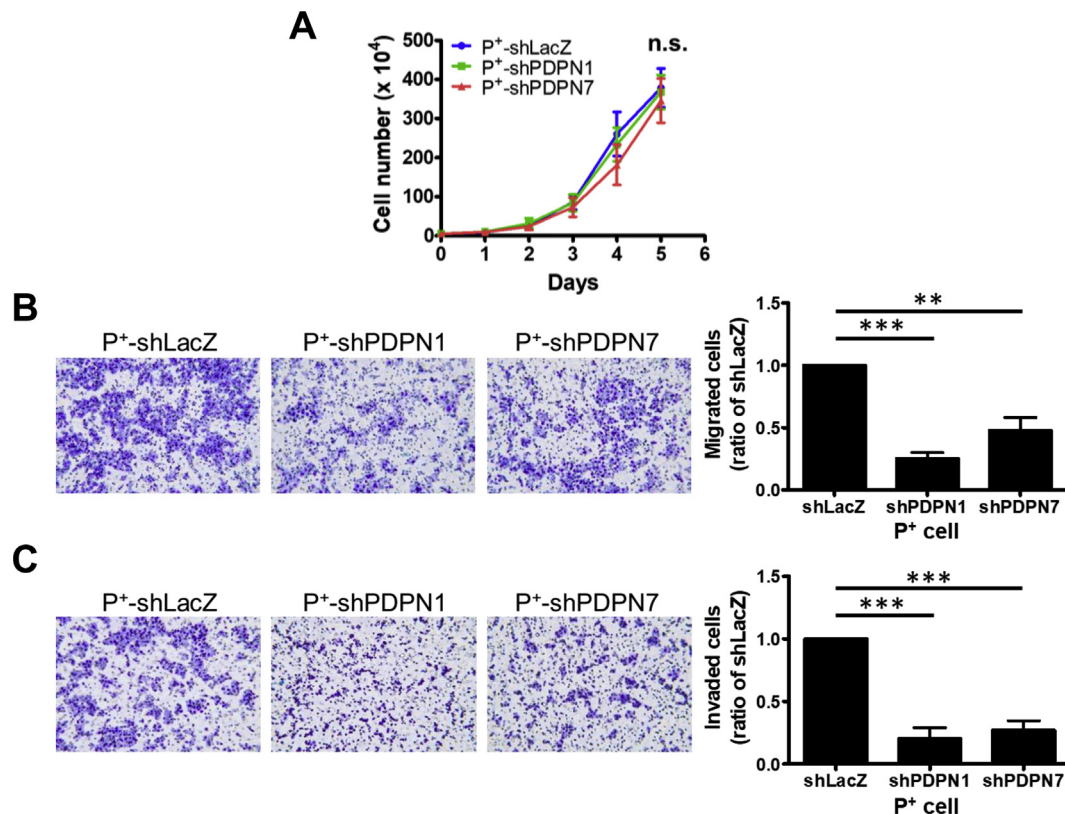

Fig. 2 **PDPN expression is crucial in promoting *in vitro* cell migration and invasion, but not cell proliferation.** (A) The cell proliferation curves of P^+-shLacZ, P^+-shPDPN1, and P^+-shPDPN7 sublines are shown. The mean ± SEM of 4 independent experiments is shown. n.s. = no significance. (B and C) Transwell migration (panel B) or invasion (panel C) assays for P^+-shLacZ, P^+-shPDPN1, and P^+-shPDPN7 sublines. Representative fields of the cells that have migrated and invaded are shown at 100X magnification (left panel of B and C). The relative number of cells that have migrated and invaded are shown with the cell number for P^+-shLacZ arbitrarily set at 1 (right panel of B and C). The mean ± SEM of 3 independent experiments is shown. **, $p < 0.01$; ***, $p < 0.001$.

shPDPN1, and P$^+$-shPDPN7 cells ($p > 0.05$) [Fig. 2A]. In the transwell migration assay, the number of P$^+$-shPDPN1 and P$^+$-shPDPN7 cells migrated through the transwell membrane was $25.2 \pm 8.2\%$ ($p < 0.001$) and $47.8 \pm 17.4\%$ ($p < 0.01$) of P$^+$-shLacZ cells, respectively [Fig. 2B]. In the transwell invasion assay, the number of P$^+$-shPDPN1 and P$^+$-shPDPN7 cells invaded through the transwell membrane was $20.3 \pm 15.0\%$ ($p < 0.001$) and $27.0 \pm 13.1\%$ ($p < 0.001$) of P$^+$-shLacZ cells, respectively [Fig. 2C]. These results indicate that PDPN expression is crucial in promoting *in vitro* cell migration and invasion but not cell proliferation.

TCIPA assay was performed to analyze whether or not PDPN expression in OECM-1 causes platelet aggregation in the absence of plasma using a platelet aggregometer. Based on our previous finding that C6-lung cells expressed PDPN and induced platelet aggregation [25], C6-lung cells were used as a positive control for TCIPA assay [Fig. 3A]. Under the same assay condition, *in vitro* platelet aggregation was not observed when human washed platelets were incubated with either P$^+$-shLacZ or P$^+$-shPDPN1 cells ([Fig. 3A], **left panel**). Increasing the cell number in the assays did not facilitate platelet aggregation induced by the sublines of OECM-1 ([Fig. 3A], **right**
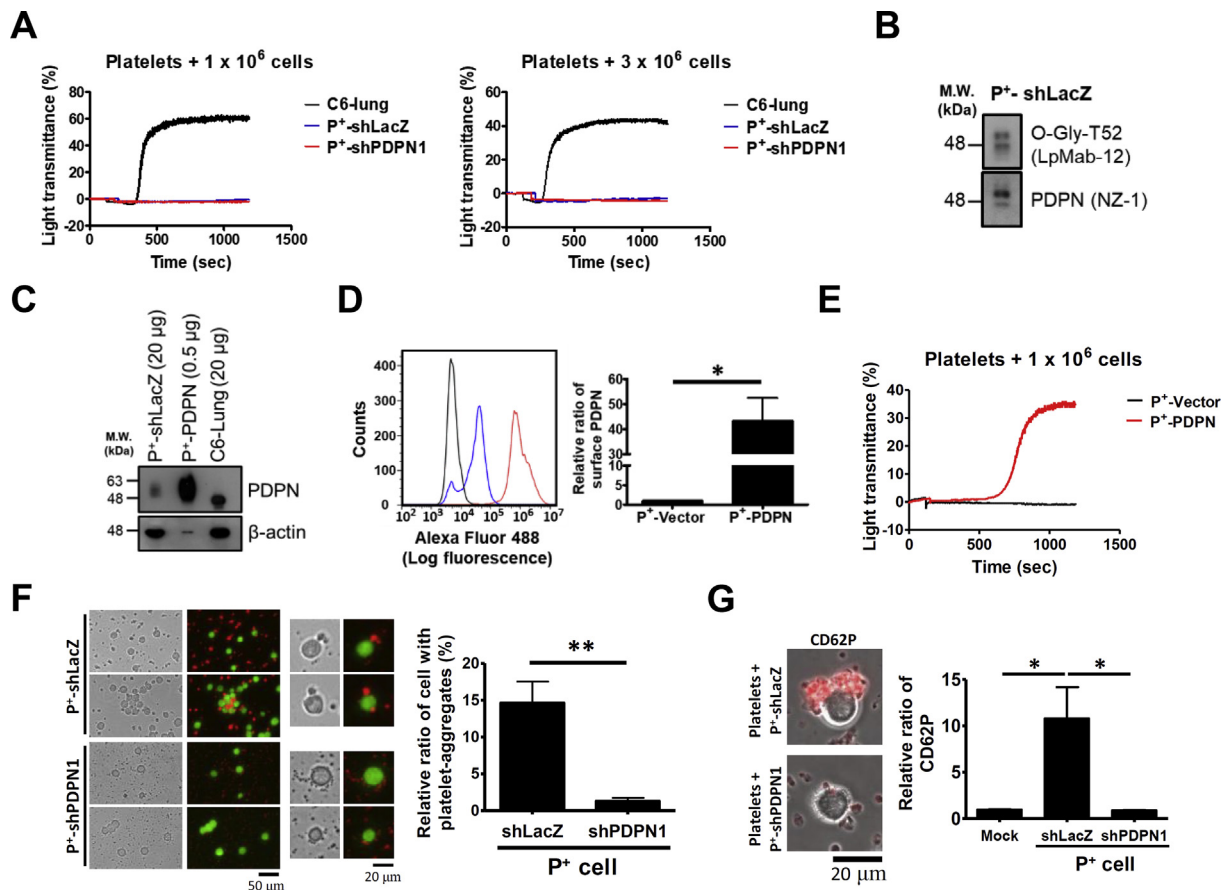

Fig. 3 **Qualitative and quantitative characterization of PDPN expression in the sublines of OECM-1 cells**. (A) The platelet aggregation assay was performed by incubation of the indicated cell lines with human washed platelets (10^9/mL). The rat C6-lung cells were used as a positive control. (B) O-Glycosylation on Thr52 of PDPN in P$^+$-shLacZ cells was detected by Western blot using the LpMab-12 antibody. (C) PDPN expression in the indicated cells was analyzed by Western blot using the rabbit anti-PDPN antibody which recognizes both human and rat PDPN. (D) P$^+$-Vector and P$^+$-PDPN cells were labeled with the Alexa Fluor 488-conjugated anti-PDPN antibody or the isotype control (incubated with P$^+$-PDPN cells) followed by flow cytometry. The histogram representing the fluorescence intensity of the indicated cells is shown (left panel). (Blue: P$^+$-Vector; red: P$^+$-PDPN; black: isotype control) The MFI was used as an indicator of PDPN expression on the cell surface. The relative ratio of surface PDPN expression is shown with PDPN expression on the cell surface of the P$^+$-Vector arbitrarily set at 1 (right panel). The mean $\pm$ SEM of 3 independent experiments is shown. *, $p < 0.05$. (E) The platelet aggregation assay was performed by incubation of the indicated cell lines with human washed platelets. (F) The platelet (calcein-orange/red) - cell (clacein-green) aggregates from the platelet aggregation assay were observed by fluorescence microscopy at 100X magnification (left panel), and the relative ratio of cell with platelet-aggregates were quantified (right panel) **, $p < 0.01$. (G) Activated platelets from the platelet aggregation assay were stained with a PE-conjugated anti-human CD62P antibody (red), and were observed by fluorescence microscopy at 1000X magnification (left panel) or flow cytometry (right panel). The MFI of CD62P in activated platelets was determined, and the relative ratio of CD62P expression is shown with its expression in resting platelets (mock) arbitrarily set at 1. The mean $\pm$ SEM of 3 independent experiments is shown. *, $p < 0.05$.

panel). Sequencing of the full-length PDPN transcripts obtained from P⁺-shLacZ cells revealed only a silent mutation at the amino acid Ser161 of PDPN (see Supplementary Fig. S2). Western blot analysis using an antibody (LpMab-12) recognizing O-glycosylated Thr52 of PDPN [33], which is crucial for human PDPN-induced platelet aggregation [30], showed that Thr52 of PDPN from P⁺-shLacZ cells underwent typical O-glycosylation [Fig. 3B]. These data indicate that gene mutation and impaired post-translational modification of Thr52 does not account for not observing platelet aggregation induced by P⁺-shLacZ cells.

Western blot analysis of the lysates from P⁺-shLacZ and C6-lung cells revealed that C6-lung cells had a four-fold higher PDPN expression when compared to the P⁺-shLacZ cells [Fig. 3C]. We therefore investigated whether the expression level of PDPN in the sublines of OECM-1 cells is critical for inducing *in vitro* platelet aggregation in the assay using aggregometer. The P⁺ sublines with PDPN overexpression (P⁺-PDPN) and its vector control cells (P⁺-Vector) were established. P⁺-PDPN cells had a significant increase in total PDPN protein when compared to the P⁺-shLacZ and C6-lung cells [Fig. 3C]. On the other hand, P⁺-PDPN cells had a 43.3-fold increase in cell surface PDPN when compared to the P⁺-Vector control cells ($p < 0.05$) [Fig. 3D]. Similar to the P⁺-shLacZ cells, P⁺-Vector control cells did not induce platelet aggregation. P⁺-PDPN cells, which expressed significant amounts of PDPN, were able to induce platelet aggregation in the assays using aggregometer [Fig. 3E]. These data indicate that a sufficient amount of PDPN expression is required for observing platelet aggregation in the aggregometer.

With the limited sensitivity of platelet aggregometer in detecting small platelet or cancer cell-platelet aggregates, TCIPA was performed by incubating fluorescence-labeled tumor cells (P⁺-shLacZ or P⁺-shPDPN1 cells) with platelets under constant stirring. The reaction mixture was then placed on a slide to examine whether there is any cancer cell-platelet mixed aggregates by fluorescence microscopy. P⁺-shLacZ cells usually caused the formation of large platelet and cancer cell-platelet aggregates. The relative ratio for cancer cells forming mixed aggregates (10 μm) with platelets was 14.6 ± 5.8% and 1.3 ± 0.9% ($p < 0.01$) for P⁺-shLacZ and P⁺-shPDPN1 cells, respectively [Fig. 3F]. Consistent with these observations, flow cytometry analysis further revealed that P⁺-shLacZ cells caused an 11.9-fold increase in platelet surface expression of CD62P when compared with the P⁺-shPDPN1 cells [Fig. 3G]. These data indicate that P⁺-shLacZ cells are able to induce platelet activation and promote the formation of cancer cells-platelets mixed aggregates.

The impact of PDPN knockdown on the overall survival of nude mice bearing ectopic xenograft OSCC tumors

An ectopic xenograft nude mouse model was established to elucidate the effects of PDPN knockdown on OSCC tumor growth and the survival of tumor-bearing mice. The P⁺-shLacZ, P⁺-shPDPN1, and P⁺-shPDPN7 cells were inoculated
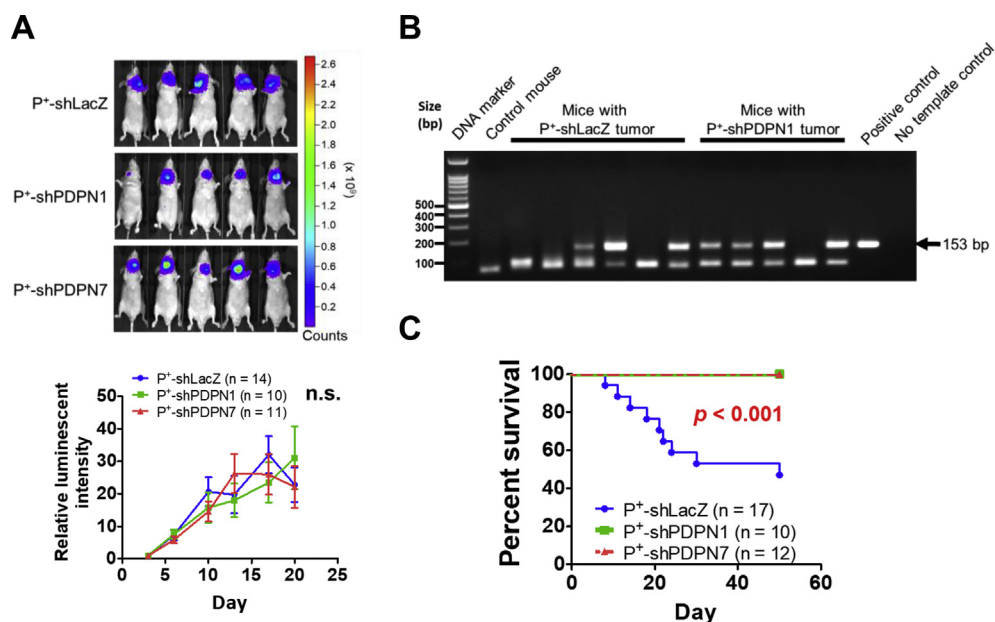

Fig. 4 **Tumor growth and overall survival of the mice bearing PDPN-knockdown OSCC tumors**. (A) Tumor size in the ectopic xenograft mouse model was measured periodically by using IVIS. Representative bioluminescence images of the mice at day 13 post-tumor cell inoculation are shown (upper panel). The relative luminescent intensity of the tumor-bearing mice was calculated and plotted (lower panel). The mean ± SEM of the indicated number of mice is shown. n.s. = no significance ($p = 0.98$). (B) CD45⁻ cells were collected from the indicated mice followed by PCR amplification of the *luciferase* gene fragment. The amplicon of the *luciferase* gene is 153 bp. The control mouse (without tumor cell inoculation) was used as the negative control for CTC isolation and detection. The genomic DNA from P⁺-shLacZ cells was used as the positive control for PCR amplification of the *luciferase* gene. No template control was a negative control for PCR amplification. (C) The survival fractions of the mice bearing P⁺-shLacZ, P⁺-shPDPN1, and P⁺-shPDPN7 tumors at the indicated time points were plotted.

into the anterior neck region of the mice, respectively, and the tumor mass was real-time monitored by IVIS. Consistent with the *in vitro* cell growth data, there was no difference in the luminescent intensity among P^+-shLacZ, P^+-shPDPN1, and P^+-shPDPN7 cells ($p > 0.05$) [Fig. 4A]. As revealed by IVIS, a common method to detect gross appearance of metastasis, all mice did not present obvious distant metastasis. Enrichment of CD45$^-$ cells from the peripheral blood followed by PCR detection of cancer cells-specific *luciferase* gene DNA fragment revealed that CTCs were present in some of the tumor-bearing mice regardless the tumors were formed by P^+-shLacZ or P^+-shPDPN1 cells [Fig. 4B]. Notably, the overall survival of the mice with P^+-shLacZ tumors was shorter than the mice with P^+-shPDPN1 and P^+-shPDPN7 tumors ($p < 0.001$). At the 50th day after inoculation of tumor cells, 47.1% (8 out of 17 mice) and 100% of the mice bearing P^+-shLacZ and P^+-shPDPN1/P^+-shPDPN7 tumors was alive, respectively [Fig. 4C]. These data indicate that PDPN is a marker for poor prognosis with minimum effect on OSCC tumor growth *in vivo*.

Effects of PDPN knockdown on intratumoral platelet infiltration, intravascular platelet aggregation and coagulation state in tumor-bearing mice

With the presence of CTCs in the bloodstream of mice [Fig. 4B] and the potential activity of PDPN in the induction of platelet aggregation, we next investigated whether platelet aggregation were visible in the tumor sections of the experimental animals. Primary tumors at 3 weeks after inoculation of

cancer cells were collected for immunofluorescence analysis of mouse platelet integrin CD41 (mCD41). A speckled staining pattern of mCD41 was defined in the PDPN-expressing P^+-shLacZ tumors [Fig. 5A, B]. The median fluorescence intensity of mCD41 in P^+-shLacZ tumors was 2.4-fold greater than the P^+-shPDPN1 and P^+-shPDPN7 tumors, which had a 73% reduction of PDPN expression. Co-immunofluorescence staining of the tumor sections with mCD41 and the endothelial cell marker mCD31 further demonstrated that mCD41 was located in the lumen of blood vessel and was also distributed intratumorally in the mice bearing P^+-shLacZ tumors [Fig. 5C].

We next investigated whether the mice inoculated with P^+-shLacZ cells had an increase in intravascular coagulation state. The platelet counts and the markers for intravascular thrombosis activity (TAT and D-dimer) were first examined. The mice bearing P^+-shLacZ, P^+-shPDPN1, and P^+-shPDPN7 tumors had comparable platelet counts [Table 2]. The median plasma levels of TAT complex and D-dimer was 13.2 ng/ml (interquartile range 11.2–22.3 ng/ml) and 7.4 ng/ml (interquartile range 7.3–8.0 ng/ml) for the mice bearing P^+-shLacZ tumors, which were significantly higher when compared to 10.0 ng/ml (interquartile range 7.3–12.1 ng/ml, $p < 0.05$) and 4.2 ng/ml (interquartile range 2.9–6.8 ng/ml, $p < 0.01$) for the mice bearing P^+-shPDPN1/P^+-shPDPN7 tumors, respectively [Fig. 6A, B].

Fibrin deposition in small blood vessels was used as another indicator for intravascular thrombosis [34]. Immunohistochemical assay was performed to analyze fibrin deposition in the pulmonary vasculature and kidney glomerulus of the mice bearing P^+-shLacZ, P^+-shPDPN1, and P^+-
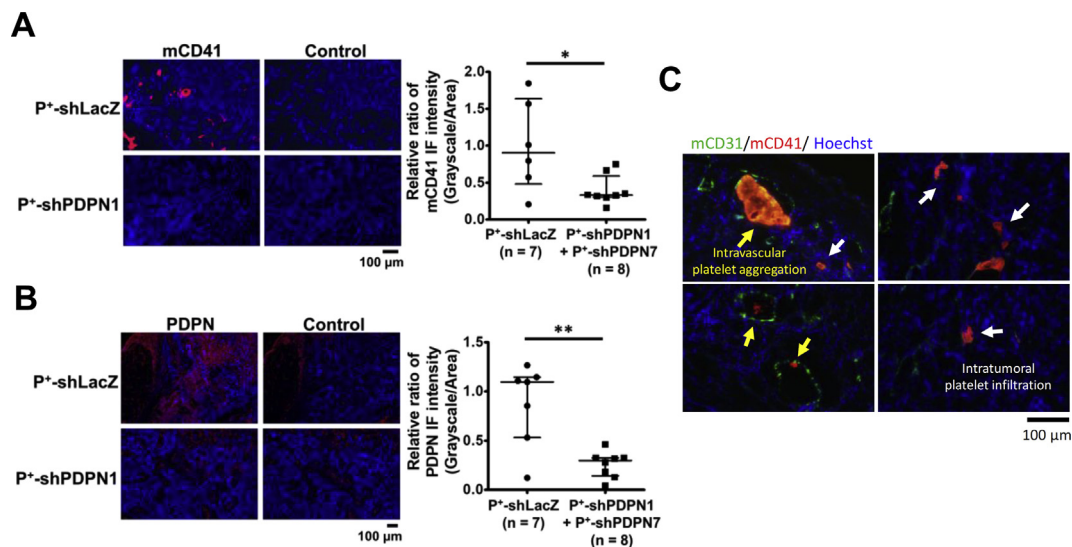

Fig. 5 **Intravascular and intratumoral mCD41 expression in nude mice bearing PDPN-positive tumors**. (A, B and C) Tumor sections were obtained from mice at day 21 after inoculation of the indicated cancer cells. The degree of immunofluorescence staining was determined by incubation with the anti-mouse platelet integrin mCD41 antibody (panel A) or anti-human PDPN antibody (panel B), followed by staining the cells with the Alexa Fluor 555-conjugated secondary antibody in the presence of Hoechst 33342 DNA staining dye (blue). The control sections represent no primary antibody-staining group. The fluorescence signal was determined by fluorescence microscopy at 100X magnification (panel A and B). Human PDPN and mCD41 expression on the tissue sections of P^+-shLacZ and P^+-shPDPN1/P^+-shPDPN7 tumors were quantified by using an IN Cell Analyzer. The median with an interquartile range for the relative ratio of mCD41 (panel A) and human PDPN (panel B) fluorescence signal per unit area of the tissue section is indicated by the horizontal lines. The mean fluorescence intensity for P^+-shLacZ tumor sections was arbitrarily set at 1.*, $p < 0.05$; **, $p < 0.01$. (C) Co-immunofluorescence staining of tumor tissue with the mouse platelet integrin mCD41 (red) and the endothelial marker mCD31 (green) in the presence of Hoechst 33342 DNA staining dye (blue). Immunofluorescence was observed by fluorescence microscopy at 200X magnification.

Table 2 The platelet counts of the mice bearing OSCC tumors.

Parameter	P+-shLacZ (n = 8)	P+-shPDPN1 (n = 4)	P+-shPDPN7 (n = 6)	*p*-value
PLT[a] (K/ml)	1098.8 ± 392.7[b]	1396.0 ± 825.5	1092.8 ± 510.6	0.755
MPV[a] (fl)	6.7 ± 0.6	6.5 ± 0.4	6.6 ± 0.3	0.721

[a] PLT: platelet; MPV: mean platelet volume.
[b] Data represents mean ± S.D.

shPDPN7 tumors. Fibrin deposition was prominently observed in the pulmonary vasculature of the mice bearing P+-shLacZ tumors (3.3 ± 0.4 pulmonary vasculature per 200X power field of the lung section) when compared to the mice bearing P+-shPDPN1/P+-shPDPN7 (1.7 ± 0.2 pulmonary vasculature per 200X power field of the lung section, $p < 0.001$) tumors [Fig. 6C]. In addition, the number of glomerulus with fibrin deposition was higher in mice bearing P+-shLacZ tumors than in mice bearing P+-shPDPN1/P+-shPDPN7 tumors [Fig. 6D]. These data indicate that the mice bearing PDPN-knockdown tumors were less susceptible to the development of intratumoral infiltration of platelet, and intravascular platelet aggregation and thrombosis.

Effects of PDPN overexpression on the overall survival, intratumoral platelet infiltration, intravascular platelet aggregation and coagulation state in tumor-bearing mice

To further investigate whether PDPN expression in the tumor cells has adverse effects on the survival of tumor-bearing mice, P− cells expressing ectopic PDPN (P−-PDPN) and vector control (P−-Vector) were established. Western blot analysis revealed that PDPN was overexpressed in P−-PDPN cells when compared to the P−-Vector cells [Fig. 7A]. The amount of cell surface PDPN in P−-PDPN cells was 222.1-fold of the P−-Vector control cells as measured by flow cytometry [Fig. 7B]. The cell growth rate of P−-PDPN cells was comparable to P−-Vector
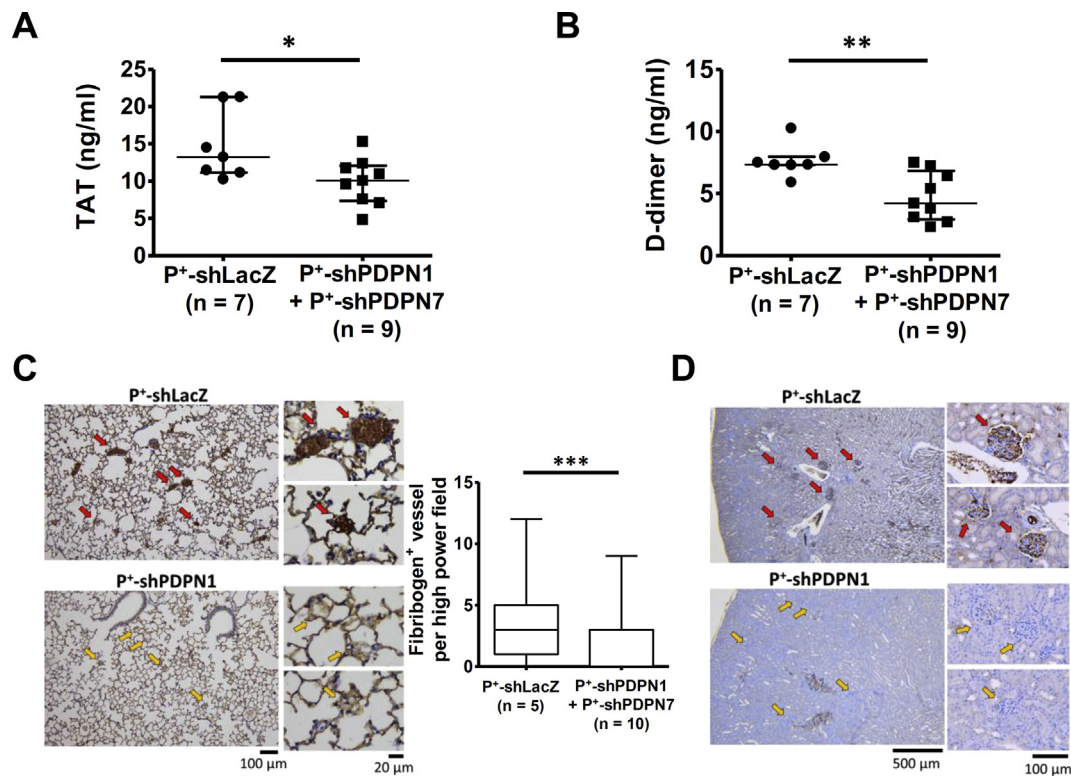

Fig. 6 **Intravascular coagulation state and fibrin(ogen) deposition were increased in the mice bearing PDPN-positive tumors.** (A and B) Plasma was collected from mice at day 50 after tumor cells were inoculated for quantifying the level of the thrombin-anti-thrombin (TAT) complex (panel A) and the D-dimer (panel B) by ELISA. The median with an interquartile range for the levels of TAT and D-dimer in mice bearing P+-shLacZ and P+- shPDPN1/P+-shPDPN7 tumors is indicated by the horizontal lines. *, $p < 0.05$; **, $p < 0.01$. (C and D) Lung (panel C) and glomerular tissue (panel D) from mice bearing P+-shLacZ and P+- shPDPN1/P+-shPDPN7 tumors were obtained at day 50 after inoculation of cancer cells and were subjected to immunohistochemical staining of fibrin(ogen). The images of the pulmonary and glomerular vasculature were observed by low and high power field light microscopy. (Red arrows: fibrin(ogen)-positive signals; yellow arrows: fibrin(ogen)-negative signals). (panel C) Boxplots represented the median (box middle line) and an interquartile range (box width) for the number of fibrin(ogen)-positive vessels in 40—50 fields (200X magnification). ***, $p < 0.001$.
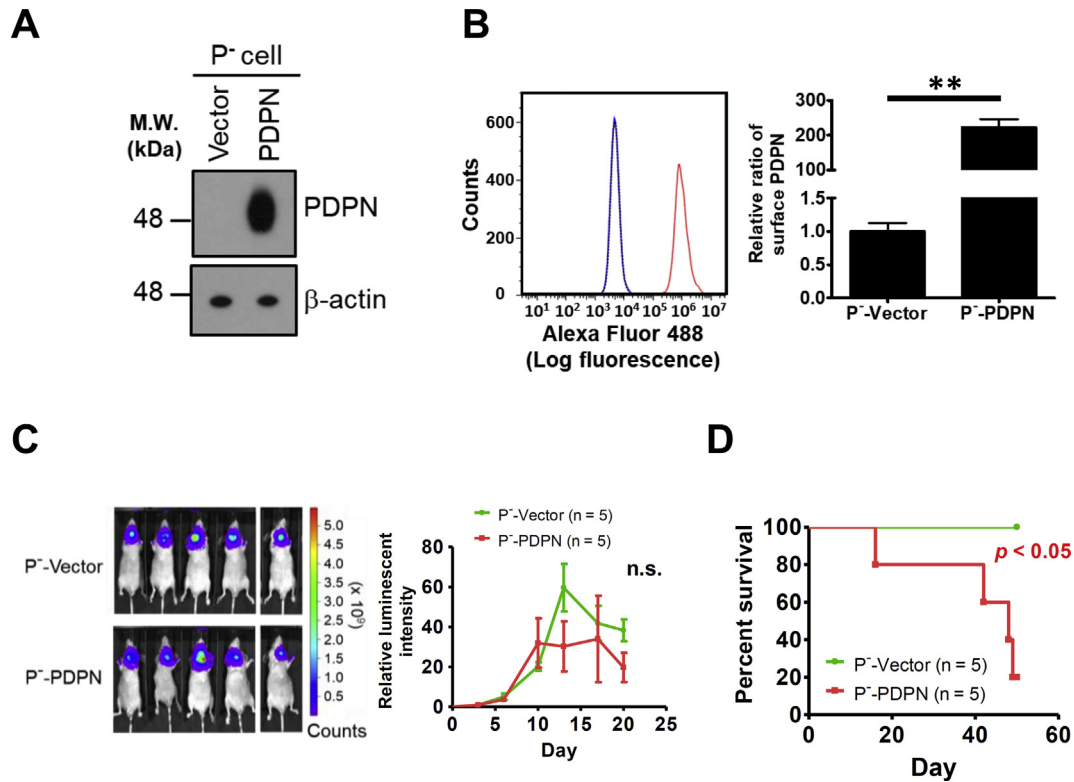
Fig. 7 **Tumor growth and overall survival of the mice bearing PDPN-overexpressing OSCC tumors**. (A) PDPN expression in the indicated cells was determined by Western blot using the anti-PDPN antibody. The expression of β-actin was used as the loading control. (B) P⁻-Vector and P⁻-PDPN cells were labeled with the Alexa Fluor 488-conjugated anti-PDPN antibody or the isotype control (incubated with P⁻-PDPN cells) followed by flow cytometry. The histogram representing the fluorescence intensity of the indicated cells is shown (left panel) (Blue: P⁻-Vector; red: P⁻-PDPN; dot line: isotype control). The MFI for the indicated cells was determined and was used as an indicator of PDPN expression on the cell surface. The relative ratio of surface PDPN expression is shown with PDPN expression on the P⁻-Vector cell surface arbitrarily set at 1 (right panel). The mean ± SEM of 3 independent experiments is shown. **, $p < 0.01$. (C) The tumor size in the ectopic xenograft mouse model was measured periodically by using IVIS. Representative bioluminescence images of the mice at day 13 post-inoculation of the tumor cells are shown (left panel). The relative luminescent intensity of the tumor-bearing mice was calculated and plotted (right panel). The mean ± SEM of the indicated number of mice is shown. n.s. = no significance ($p = 0.42$). (D) The survival fraction of the mice bearing P⁻-Vector and P⁻-PDPN tumors at the indicated time points.

cells (see Supplementary Fig. S3A). P⁻-PDPN cells expressed a significant amount of PDPN and therefore were able to induce platelet aggregation *in vitro* in the platelet aggregometer assay (see Supplementary Fig. S3B).

To elucidate the effects of PDPN overexpression on OSCC tumor growth and the survival of tumor-bearing mice, the P⁻-Vector and P⁻-PDPN cells were inoculated into the anterior neck region of the mice, respectively. The tumor mass was real-time monitored by IVIS. There was no difference in the luminescent intensity among P⁻-Vector and P⁻-PDPN tumors ($p > 0.05$) [Fig. 7C]. Consistent with the data of P⁺ cells [Fig. 4C], the overall survival of the mice bearing P⁻-PDPN tumors was shorter than the mice with P⁻-Vector tumors ($p < 0.05$). At the 50th day after inoculation of tumor cells, 20% (1 out of 5 mice) and 100% of the mice bearing P⁻-PDPN and P⁻-Vector tumors was alive, respectively [Fig. 7D].

Similar to the findings of P⁺-shLacZ tumors, a speckled staining pattern of mCD41 indicating platelet aggregation was also defined in the P⁻-PDPN tumor sections [Fig. 8A]. The median fluorescence intensity of mCD41 in P⁻-PDPN tumors was 8.3-fold greater than the P⁻-Vector tumors [Fig. 8B]. Co-immunofluorescence staining of the tumor sections with mCD41 and the endothelial cell marker mCD31 further demonstrated that mCD41 was located in the lumen of blood vessel and was also distributed intra-tumorally in the mice bearing P⁻-PDPN tumors [Fig. 8C]. The plasma levels of TAT complex and D-dimer and fibrin deposition in the pulmonary vasculature and kidney glomerulus of the mice bearing P⁻-PDPN and P⁻-Vector tumors were also examined [Fig. 9]. The plasma levels of TAT but not D-dimer and the number of pulmonary vasculature with fibrin deposition were slightly increased, although not statistically significant, in the mice bearing
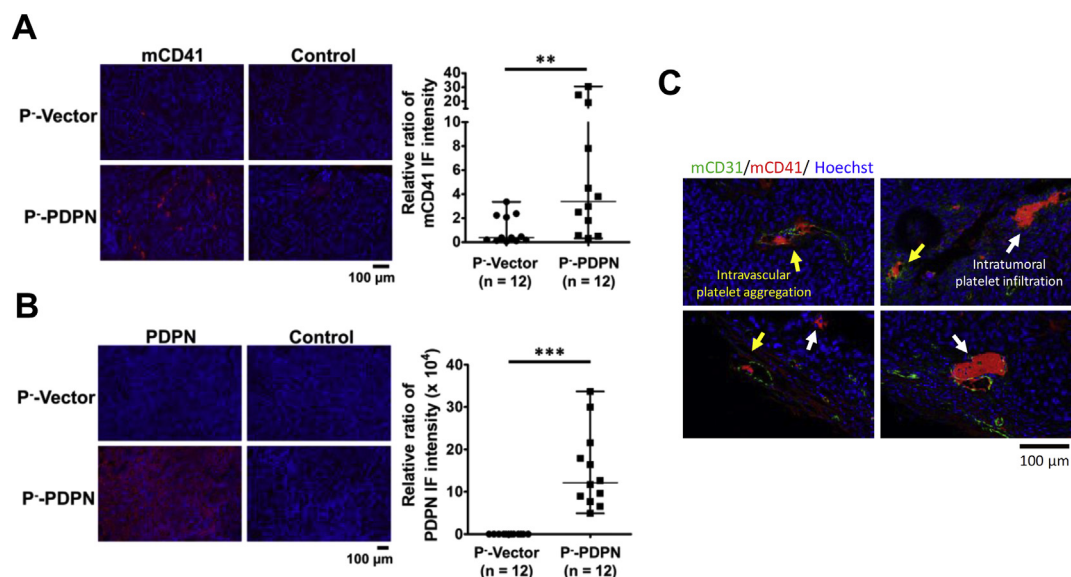
Fig. 8 **Intravascular and intratumoral mCD41 expression in nude mice bearing PDPN-overexpression tumors**. (A, B and C) Tumor sections were obtained from mice at day 21 after inoculation of the indicated cancer cells. The degree of immunofluorescence staining was determined by incubation with the anti-mouse platelet integrin mCD41 antibody (panel A) or anti-human PDPN antibody (panel B), followed by staining the cells with the Alexa Fluor 555-conjugated secondary antibody in the presence of Hoechst 33342 DNA staining dye (blue). The control sections represent no primary antibody-staining group. The fluorescence signal was determined by fluorescence microscopy at 100X magnification (panel A and B). Human PDPN and mCD41 expression on the tissue sections of P⁻-Vector and P⁻-PDPN tumors were quantified by using an IN Cell Analyzer. The median with an interquartile range for the relative ratio of mCD41 (panel A) and human PDPN (panel B) fluorescence signal per unit area of the tissue section is indicated by the horizontal lines. The mean fluorescence intensity for P⁻-Vector tumor sections was arbitrarily set at 1. **, $p < 0.01$; ***, $p < 0.001$. (C) Co-immunofluorescence staining of tumor tissue with the mouse platelet integrin mCD41 (red) and the endothelial marker mCD31 (green) in the presence of Hoechst 33342 DNA staining dye (blue). Immunofluorescence was observed by fluorescence microscopy at 200X magnification.

P⁻-PDPN tumors when compared to the mice bearing P⁻-Vector tumors.

Discussion

PDPN is implicated as a marker of poor prognosis in patients with OSCC and attributed as an oncogene by promoting *in vitro* cancer cell growth, migration, invasion, and epithelial-mesenchymal transition [5]. An animal model by inoculating OECM-1 cells on the anterior neck region of mouse was established in this study to unveil that, in contrast to the conception revealed by this and most prior *in vitro* studies [13,35], PDPN does not contribute to *in vivo* tumor growth and distant metastasis of OSCC cells. Oral cancer cells with PDPN expression instead cause an increase in intravascular platelet aggregation and, through unknown mechanisms, the infiltration of platelets or platelet-related components to the extravascular tumor environment. The aforementioned effects are correlated to the unfavorable overall survival of the animals. These findings provide a link between PDPN-expressing OSCC and thrombotic risk and lay the foundation for uncovering novel molecular basis for the pathophysiology of OSCC.

In this study, nearly 50% of the mice bearing P⁺-shLacZ tumors died within 50 days after inoculation of cancer cells. All mice bearing P⁺-shPDPN1 or P⁺-shPDPN7 tumors were

alive during the same period of time. Consistent with these observations, 80% of the mice bearing P⁻-PDPN tumors died within 50 days after inoculation of cancer cells, while all mice bearing P⁻-Vector tumors were alive. These observations are consistent with the data obtained from clinical studies which revealed that PDPN expression correlates with mortality in OSCC patients [20,21]. The five year overall survival and disease free survival for patients with tumors with undetectable PDPN expression was 86% and 100%, while for patients with tumors exhibiting high PDPN expression was 23% and 37%, respectively [5]. The animal model as reported herein represents a suitable model to investigate the pathophysiology of OSCC.

Most previous studies focused on analyzing PDPN function in the cellular properties and malignant progression of OSCC and demonstrated that PDPN mainly regulates cancer cell migration and invasion [13,35]. The potential functions of PDPN in inducing platelet aggregation and thrombus formation have been mostly overlooked and were not analyzed. In this study, we comprehensively analyzed and addressed the effects of PDPN expression on both malignant progression and cancer-associated thrombosis using *in vitro* and *in vivo* approaches. Based on the data reported in this study, we demonstrated for the first time that the mice bearing OSCC tumors exhibiting high PDPN expression is associated with the development of intravascular platelet aggregation and thrombosis that may contribute to the unfavorable survival of
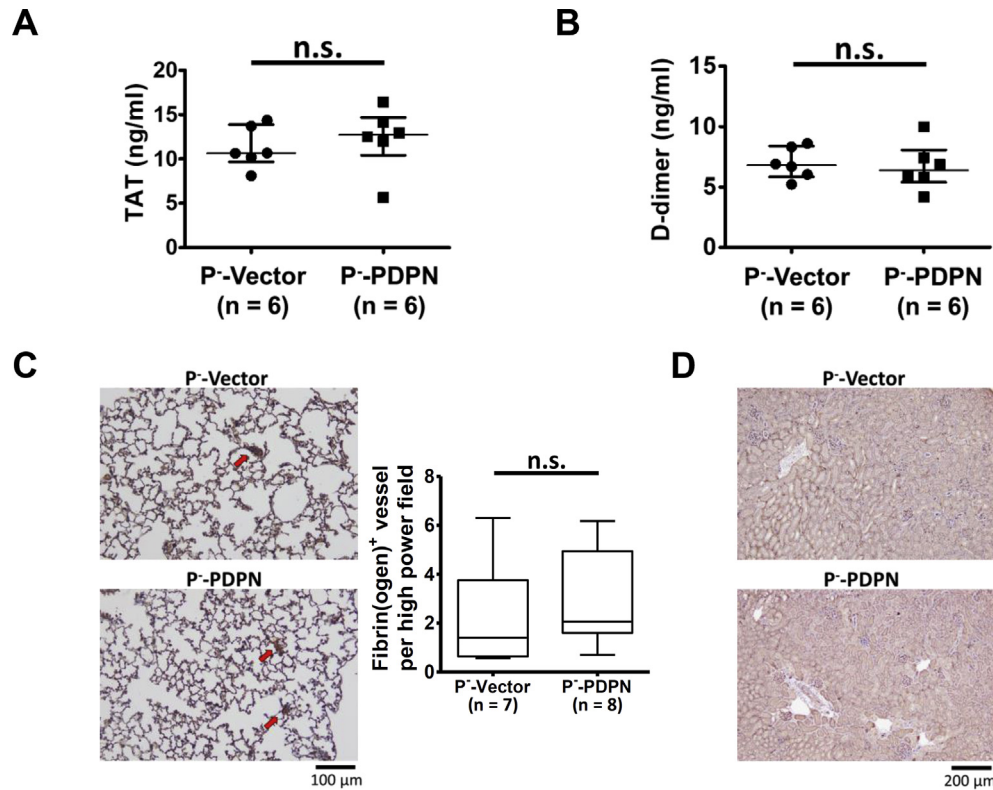
Fig. 9 **Intravascular coagulation state and fibrin(ogen) deposition were comparable between the mice bearing the P⁻-Vector and P⁻-PDPN tumors**. (A and B) Plasma was collected from mice at day 50 after tumor cell inoculation for quantifying the levels of thrombin-anti-thrombin (TAT) complex (panel A) and D-dimer (panel B) by ELISA. The median with an interquartile range for the levels of TAT and D-dimer in the mice bearing P⁻-Vector and P⁻-PDPN tumors is indicated by the horizontal lines. (C and D) Lung (panel C) and glomerular tissue (panel D) from mice bearing the P⁻-Vector and P⁻-PDPN tumors that were obtained at day 50 after inoculation of cancer cells and were subjected to immunohistochemical staining of fibrin(ogen). The images of the pulmonary and glomerular vasculature were observed by low and high power field light microscopy. (Red arrows: fibrin(ogen)-positive signals). (panel C) Boxplots represented the median (box middle line) and an interquartile range (box width) for the number of fibrin(ogen)-positive vessels in 10 fields of each lung section (200X magnification).

the mice. This notion is supported by several lines of evidence. First, distant metastasis was not occurred in the mice with P⁺-shLacZ tumors. Second, platelet aggregation as observed by immunofluorescence staining of mCD41 were more often present in the blood vessel of the mice bearing P⁺-shLacZ tumors when compared to the mice with P⁺-shPDPN1 or P⁺-shPDPN7 tumors. Third, the plasma levels of D-dimer and TAT, the markers for assessing thrombosis within the bloodstream [36], were higher in the mice bearing P⁺-shLacZ tumors when compared with the mice bearing P⁺-shPDPN1 or P⁺-shPDPN7 tumors. Fourth, fibrin deposition was increased in the pulmonary vasculature and kidney glomerulus of the mice bearing P⁺-shLacZ tumors. Fifth, mice bearing P⁺-shLacZ tumors had a shorter overall survival and died suddenly without any sign of weakness and weight loss (data not shown). These findings fill the gap of previous studies by linking PDPN expression and cancer-associated thrombosis and implicate that PDPN expression is related to the occurrence of hemostatic imbalance in patients with OSCC. These findings are also in accord with the notion that cancer-associated thrombosis is one of the major cause of morbidity and mortality in patients with cancer [37], with about 15–20% of cancer

patients diagnosed with venous thromboembolism (VTE) [38] and 26.3% of OSCC patients diagnosed with VTE after major oral and maxillofacial surgery [39]. Increased concentration of fibrin degradation products is also detected in the serum of patients with advanced stage of OSCC when compares to the normal individuals [40]. Consistent with these notions, the synthetic small molecule compound 2CP which has been shown to disrupt PDPN and platelet CLEC-2 interaction [25] prolonged the overall survival of mice bearing P⁺-shLacZ tumors (unpublished data). PDPN in the tumor cells may thereby be considered as a contributing factor for development of cancer-associated thrombosis. According to the findings reported in this and other studies [24,35], PDPN elicits dual effects by inducing cancer-associated thrombosis and malignant progression that account for the aggressive phenotype associated with OSCC tumors exhibiting high PDPN expression.

How tumors with PDPN expression induce cancer-associated thrombosis is another issue that needs to be addressed. CTCs with or without PDPN expression are presented in the peripheral blood of patients with oral cancer [21]. Similar to the data of clinical studies, CTCs are presented in

the peripheral blood of the mice bearing either P$^+$-shLacZ or P$^+$-shPDPN1 tumors. However, thrombus formation prominently occurs only in the mice with P$^+$-shLacZ tumors. It is likely that CTCs from the P$^+$-shLacZ tumors interact directly with and activate platelets leading to the development of thrombosis. This is supported by our findings that P$^+$-shLacZ cells interact with platelet leading to platelet activation, surface expression of CD62P and formation of cancer cell-platelet mixed aggregates. Alternatively, exosomes released by tumor cells might contribute to platelet activation and aggregation. In this regard, exosomes with tissue factor (TF) expression are released by breast cancer cells to stimulate platelet aggregation [41]. Exosomes with PDPN expression are released by MDCK cells to participate in the induction of lymphatic vessel formation [42]. We also found that PDPN is presented in the exosomes released by P$^+$-shLacZ cells *in vitro* (data not shown). Whether P$^+$-shLacZ tumors released exosomes with PDPN expression thereby providing an additional route to stimulate platelet activation and thrombus formation remains to be elucidated.

Platelet infiltration into solid tumors is known to facilitate tumor growth and aggressiveness [22,43]. We have noted that the immunofluorescence staining signal of platelet integrin mCD41 is present not only in the blood vessel but also in the extravascular tumor environment of the P$^+$-shLacZ tumors. The extravascular/intratumoral signal of mCD41 is likely caused by platelet extravasation through the highly permeable tumor blood vessels [44]. Several platelet proteins including focal adhesion kinase and platelet factor 4 have been implicated in platelet accumulation at tumor site [45,46]. Platelet aggregation was induced when platelets encountered by tumor cells expressing PDPN. Alternatively, the extravascular/intratumoral signal of mCD41 may represent the components released by platelets such as microparticles and/or exosomes. Platelet microparticles have been shown to present at the tumor site and promote cancer progression by transforming cells into an aggressive phenotype [47] and disseminating tumor cells into the peripheral blood [22]. Miyata et al. reported that intratumoral platelet aggregates found in the tumor mass of PDPN-expressing lung cancer were related to the growth of tumor cells [48]. Unlike their findings, platelet aggregates at the tumor site as reported in this study did not seem to correlate with tumor growth of OSCC cells. Whether the functional roles of the extravascular/intratumoral platelet aggregates are cancer type-specific is worthy to be investigated further.

We have noted that, unlike the mice bearing tumors derived from P$^+$-shLacZ cells, the plasma levels of thrombotic markers and fibrin(ogen) deposition in lung were not significantly increased in the mice bearing P$^-$-PDPN tumors. The discrepancy between these data has raised a question of whether PDPN regulates these thrombosis-relative factors. P$^+$ and P$^-$ cells were derived from different populations of OECM-1. PDPN may cooperate with an undefined molecule that is present in P$^+$-shLacZ cells but not P$^-$-PDPN cells to activate the coagulation cascade in the mice bearing PDPN-positive tumors. Alternatively, other proteins regulate coagulation activation independent of PDPN leading to the increase in plasma D-dimer and TAT, and fibrin deposition in the blood vessels. In this regard, TF is a candidate protein with functions

in hemostasis and thrombosis. TF expression in tumor cells is associated with the occurrence of VTE in cancer patients [49] and phosphatidylserine acts synergistically with TF leading to robust thrombin formation [50]. Hence, in addition to causing intratumoral platelet infiltration and intravascular platelet aggregation, whether and how PDPN regulates the thrombotic activity associated with coagulation activation and fibrin(ogen) deposition and whether co-expression of PDPN and TF in cancer cells is associated with a higher risk of VTE remain to be elucidate.

Conclusions

Understanding the molecular basis for cancer-associated thrombosis is an emerging issue for investigation. This study demonstrates for the first time in a mice model that PDPN expression in the OSCC tumors activates platelet activation and promotes intravascular platelet aggregation and intratumoral platelet infiltration which consequently leads to an increase in coagulation state and a decrease in overall survival of the mice bearing tumors with PDPN expression. This study provides new insights into PDPN function in cancer-associated thrombosis and its role in the pathophysiology of OSCC.

Funding

Conflicts of interest

The authors declare no competing interests.

Acknowledgements

Appendix A. Supplementary data

Supplementary data to this article can be found online at https://doi.org/10.1016/j.bj.2019.07.001.

REFERENCES

[1] Shield KD, Ferlay J, Jemal A, Sankaranarayanan R, Chaturvedi AK, Bray F, et al. The global incidence of lip, oral cavity, and pharyngeal cancers by subsite in 2012. CA Cancer J Clin 2017;67:51—64.

[2] Sano D, Myers JN. Metastasis of squamous cell carcinoma of the oral tongue. Cancer Metastasis Rev 2007;26:645—62.

[3] Kunita A, Kashima TG, Morishita Y, Fukayama M, Kato Y, Tsuruo T, et al. The platelet aggregation-inducing factor aggrus/podoplanin promotes pulmonary metastasis. Am J Pathol 2007;170:1337—47.

[4] Suzuki-Inoue K, Kato Y, Inoue O, Kaneko MK, Mishima K, Yatomi Y, et al. Involvement of the snake toxin receptor CLEC-2, in podoplanin-mediated platelet activation, by cancer cells. J Biol Chem 2007;282:25993—6001.

[5] Retzbach EP, Sheehan SA, Nevel EM, Batra A, Phi T, Nguyen ATP, et al. Podoplanin emerges as a functionally relevant oral cancer biomarker and therapeutic target. Oral Oncol 2018;78:126—36.

[6] Osada M, Inoue O, Ding G, Shirai T, Ichise H, Hirayama K, et al. Platelet activation receptor CLEC-2 regulates blood/lymphatic vessel separation by inhibiting proliferation, migration, and tube formation of lymphatic endothelial cells. J Biol Chem 2012;287:22241—52.

[7] Lowe KL, Finney BA, Deppermann C, Hagerling R, Gazit SL, Frampton J, et al. Podoplanin and CLEC-2 drive cerebrovascular patterning and integrity during development. Blood 2015;125:3769—77.

[8] Herzog BH, Fu J, Wilson SJ, Hess PR, Sen A, McDaniel JM, et al. Podoplanin maintains high endothelial venule integrity by interacting with platelet CLEC-2. Nature 2013;502:105—9.

[9] Tamura S, Suzuki-Inoue K, Tsukiji N, Shirai T, Sasaki T, Osada M, et al. Podoplanin-positive periarteriolar stromal cells promote megakaryocyte growth and proplatelet formation in mice by CLEC-2. Blood 2016;127:1701—10.

[10] Honma M, Minami-Hori M, Takahashi H, Iizuka H. Podoplanin expression in wound and hyperproliferative psoriatic epidermis: regulation by TGF-beta and STAT-3 activating cytokines, IFN-gamma, IL-6, and IL-22. J Dermatol Sci 2012;65:134—40.

[11] Kumar V, Dasoveanu DC, Chyou S, Tzeng TC, Rozo C, Liang Y, et al. A dendritic-cell-stromal axis maintains immune responses in lymph nodes. Immunity 2015;42:719—30.

[12] Dang Q, Liu J, Li J, Sun Y. Podoplanin: a novel regulator of tumor invasion and metastasis. Med Oncol 2014;31:24.

[13] Li YY, Zhou CX, Gao Y. Podoplanin promotes the invasion of oral squamous cell carcinoma in coordination with MT1-MMP and Rho GTPases. Am J Cancer Res 2015;5:514—29.

[14] Martin-Villar E, Megias D, Castel S, Yurrita MM, Vilaro S, Quintanilla M. Podoplanin binds ERM proteins to activate RhoA and promote epithelial-mesenchymal transition. J Cell Sci 2006;119:4541—53.

[15] Tsuneki M, Yamazaki M, Maruyama S, Cheng J, Saku T. Podoplanin-mediated cell adhesion through extracellular matrix in oral squamous cell carcinoma. Lab Investig 2013;93:921—32.

[16] Hwang YS, Xianglan Z, Park KK, Chung WY. Functional invadopodia formation through stabilization of the PDPN transcript by IMP-3 and cancer-stromal crosstalk for PDPN expression. Carcinogenesis 2012;33:2135—46.

[17] Cueni LN, Hegyi I, Shin JW, Albinger-Hegyi A, Gruber S, Kunstfeld R, et al. Tumor lymphangiogenesis and metastasis to lymph nodes induced by cancer cell expression of podoplanin. Am J Pathol 2010;177:1004—16.

[18] Vormittag L, Thurnher D, Geleff S, Pammer J, Heiduschka G, Brunner M, et al. Co-expression of Bmi-1 and podoplanin predicts overall survival in patients with squamous cell carcinoma of the head and neck treated with radio(chemo)therapy. Int J Radiat Oncol Biol Phys 2009;73:913—8.

[19] Yuan P, Temam S, El-Naggar A, Zhou X, Liu DD, Lee JJ, et al. Overexpression of podoplanin in oral cancer and its association with poor clinical outcome. Cancer 2006;107:563—9.

[20] Kreppel M, Scheer M, Drebber U, Ritter L, Zoller JE. Impact of podoplanin expression in oral squamous cell carcinoma: clinical and histopathologic correlations. Virchows Arch 2010;456:473—82.

[21] Hsieh JC, Lin HC, Huang CY, Hsu HL, Wu TM, Lee CL, et al. Prognostic value of circulating tumor cells with podoplanin expression in patients with locally advanced or metastatic head and neck squamous cell carcinoma. Head Neck 2015;37:1448—55.

[22] Yan M, Jurasz P. The role of platelets in the tumor microenvironment: from solid tumors to leukemia. Biochim Biophys Acta 2016;1863:392—400.

[23] Cueni LN, Chen L, Zhang H, Marino D, Huggenberger R, Alitalo A, et al. Podoplanin-Fc reduces lymphatic vessel formation in vitro and in vivo and causes disseminated intravascular coagulation when transgenically expressed in the skin. Blood 2010;116:4376—84.

[24] Riedl J, Preusser M, Nazari PM, Posch F, Panzer S, Marosi C, et al. Podoplanin expression in primary brain tumors induces platelet aggregation and increases risk of venous thromboembolism. Blood 2017;129:1831—9.

[25] Chang YW, Hsieh PW, Chang YT, Lu MH, Huang TF, Chong KY, et al. Identification of a novel platelet antagonist that binds to CLEC-2 and suppresses podoplanin-induced platelet aggregation and cancer metastasis. Oncotarget 2015;6:42733—48.

[26] Tsai HJ, Chien KY, Liao HR, Shih MS, Lin YC, Chang YW, et al. Functional links between Disabled-2 Ser723 phosphorylation and thrombin signaling in human platelets. J Thromb Haemost 2017;15:2029—44.

[27] Hung WS, Ling P, Cheng JC, Chang SS, Tseng CP. Disabled-2 is a negative immune regulator of lipopolysaccharide-stimulated Toll-like receptor 4 internalization and signaling. Sci Rep 2016;6:35343.

[28] Lin HC, Hsu HC, Hsieh CH, Wang HM, Huang CY, Wu MH, et al. A negative selection system PowerMag for effective leukocyte depletion and enhanced detection of EpCAM positive and negative circulating tumor cells. Clin Chim Acta 2013;419:77—84.

[29] Krishnan H, Ochoa-Alvarez JA, Shen Y, Nevel E, Lakshminarayanan M, Williams MC, et al. Serines in the intracellular tail of podoplanin (PDPN) regulate cell motility. J Biol Chem 2013;288:12215—21.

[30] Kaneko MK, Kato Y, Kameyama A, Ito H, Kuno A, Hirabayashi J, et al. Functional glycosylation of human podoplanin: glycan structure of platelet aggregation-inducing factor. FEBS Lett 2007;581:331—6.

[31] Cheng CY, Liu CJ, Huang YC, Wu SH, Fang HW, Chen YJ. BI2536 induces mitotic catastrophe and radiosensitization in human oral cancer cells. Oncotarget 2018;9:21231—43.

[32] Chiang CH, Wu CC, Lee LY, Li YC, Liu HP, Hsu CW, et al. Proteomics analysis reveals involvement of Krt17 in areca nut-induced oral carcinogenesis. J Proteome Res 2016;15:2981—97.

[33] Kato Y, Ogasawara S, Oki H, Goichberg P, Honma R, Fujii Y, et al. LpMab-12 established by CasMab technology specifically detects sialylated O-glycan on Thr52 of platelet aggregation-stimulating domain of human podoplanin. PLoS One 2016;11:e0152912.

[34] Sun DS, Chang YC, Lien TS, King CC, Shih YL, Huang HS, et al. Endothelial cell sensitization by death receptor fractions of an anti-dengue nonstructural protein 1 antibody induced plasma leakage, coagulopathy, and mortality in mice. J Immunol 2015;195:2743–53.

[35] Inoue H, Miyazaki Y, Kikuchi K, Yoshida N, Ide F, Ohmori Y, et al. Podoplanin promotes cell migration via the EGF-Src-Cas pathway in oral squamous cell carcinoma cell lines. J Oral Sci 2012;54:241–50.

[36] Geddings JE, Mackman N. Tumor-derived tissue factor-positive microparticles and venous thrombosis in cancer patients. Blood 2013;122:1873–80.

[37] Elyamany G, Alzahrani AM, Bukhary E. Cancer-associated thrombosis: an overview. Clin Med Insights Oncol 2014;8:129–37.

[38] Lee AY. Management of thrombosis in cancer: primary prevention and secondary prophylaxis. Br J Haematol 2005;128:291–302.

[39] Stein PD, Beemath A, Meyers FA, Skaf E, Sanchez J, Olson RE. Incidence of venous thromboembolism in patients hospitalized with cancer. Am J Med 2006;119:60–8.

[40] Gharat L, Rathod GP, Kandalgaonkar S. Quantitative estimation of serum fibrinogen degradation product levels in oral premalignant and malignant lesions. J Int Oral Health 2013;5:65–72.

[41] Gomes FG, Sandim V, Almeida VH, Rondon AMR, Succar BB, Hottz ED, et al. Breast-cancer extracellular vesicles induce platelet activation and aggregation by tissue factor-independent and -dependent mechanisms. Thromb Res 2017;159:24–32.

[42] Carrasco-Ramirez P, Greening DW, Andres G, Gopal SK, Martin-Villar E, Renart J, et al. Podoplanin is a component of extracellular vesicles that reprograms cell-derived exosomal proteins and modulates lymphatic vessel formation. Oncotarget 2016;7:16070–89.

[43] Costa B, Eisemann T, Strelau J, Spaan I, Korshunov A, Liu HK, et al. Intratumoral platelet aggregate formation in a murine preclinical glioma model depends on podoplanin expression on tumor cells. Blood Adv 2019;3:1092–102.

[44] Van den Brenk HA, Crowe M, Kelly H, Stone MG. The significance of free blood in liquid and solid tumours. Br J Exp Pathol 1977;58:147–59.

[45] Haemmerle M, Bottsford-Miller J, Pradeep S, Taylor ML, Choi HJ, Hansen JM, et al. FAK regulates platelet extravasation and tumor growth after antiangiogenic therapy withdrawal. J Clin Investig 2016;126:1885–96.

[46] Pucci F, Rickelt S, Newton AP, Garris C, Nunes E, Evavold C, et al. PF4 promotes platelet production and lung cancer growth. Cell Rep 2016;17:1764–72.

[47] Grande R, Dovizio M, Marcone S, Szklanna PB, Bruno A, Ebhardt HA, et al. Platelet-derived microparticles from obese individuals: characterization of number, size, proteomics, and crosstalk with cancer and endothelial cells. Front Pharmacol 2019;10:7.

[48] Miyata K, Takemoto A, Okumura S, Nishio M, Fujita N. Podoplanin enhances lung cancer cell growth in vivo by inducing platelet aggregation. Sci Rep 2017;7:4059.

[49] Rondon AMR, Kroone C, Kapteijn MY, Versteeg HH, Buijs JT. Role of tissue factor in tumor progression and cancer-associated thrombosis. Semin Thromb Hemost 2019;45:396–412.

[50] Fernandes RS, Kirszberg C, Rumjanek VM, Monteiro RQ. On the molecular mechanisms for the highly procoagulant pattern of C6 glioma cells. J Thromb Haemost 2006;4:1546–52.